by Clayton R. Paul

# Modeling electromagnetic interference properties of printed circuit boards

The mathematical modeling of a printed circuit board (PCB) for the prediction of its electromagnetic interference (EMI) properties is investigated. Two key aspects examined are crosstalk and the high-frequency voltage developed between the ends of a PCB land (ground drop). The notion of partial inductance as opposed to loop inductance is the key to predicting the high-frequency voltages that are developed between two ends of a land. Crosstalk predictions are a by-product of the modeling. Experimental results are shown to illustrate the accuracy of the model. A technique for the accurate measurement of the highfrequency voltage developed between two ends of a PCB land is described and explained in terms of partial inductances.

### 1. Introduction

Electronic systems are becoming increasingly complex in terms of numbers and density of components as well as in

<sup>®</sup>Copyright 1989 by International Business Machines Corporation. Copying in printed form for private use is permitted without payment of royalty provided that (1) each reproduction is done without alteration and (2) the *Journal* reference and IBM copyright notice are included on the first page. The title and abstract, but no other portions, of this paper may be copied or distributed royalty free without further permission by computer-based and other information-service systems. Permission to *republish* any other portion of this paper must be obtained from the Editor.

function. An important problem associated with these technological advancements is the increasing potential for a system to cause electromagnetic interference (EMI) with other electronic systems. In order to address this problem, the Federal Communications Commission (FCC) in the United States published under FCC Rules and Regulations, Part 15, Subpart J, the requirement that any commercial product marketed in the United States that "generates and uses timing signals or pulses at a rate in excess of 10,000 pulses (cycles) per second and uses digital techniques" must not radiate signals in excess of certain levels in the frequency range of 30 MHz to 1 GHz [1]. A similar requirement is imposed on emissions conducted from the product into the commercial power mains in the frequency range of 450 kHz to 30 MHz. Clock frequencies in digital electronic products are well in excess of 10 kHz, so that virtually all digital products today are subject to the FCC regulations. Products that are intended to be marketed in other countries are subject to similar and no less stringent regulations. These regulations are intended to limit the interference caused by electromagnetic emissions from the product. Susceptibility of the product to external electromagnetic emissions from other products is not currently regulated by governmental agencies, although the FCC has been granted the authority to do so. However, companies usually voluntarily test their products for susceptibility in order to ensure that the product will operate satisfactorily in the expected environment.

These governmental restrictions on the electromagnetic emissions of a product have caused considerable concern in the electronics industry, since a product cannot be legally marketed in a country unless the product's electromagnetic emissions comply with that country's regulatory limits. Companies that produce these electronic products currently devote significant resources to designing their products to satisfy not only these legal requirements but also susceptibility requirements. When a product is tested and found not to be in compliance with these requirements, suppression components must be added to the product in order to bring it into compliance. This adds cost to the product over that required for its desired functional performance. This also frequently results in schedule delays that are required to diagnose the source of the emission (or susceptibility). Therefore, the design of a product to minimize its electromagnetic emissions (and its susceptibility to electromagnetic emissions) is an important aspect of its design.

The subject of this paper is the mathematical modeling of printed circuit boards (PCBs) with regard to the prediction of the EMI properties of the board. It is known that two different layouts or positionings of the board's conductors (lands) can yield vastly different radiated and conducted emission profiles of the product that contains the board [2, 3]. Therefore, an understanding of how different land patterns affect the EMI properties of the board (and consequently the product) is an important aspect in controlling the EMI properties of the product. PCBs are also connected to peripheral devices with cables. These cables serve as effective radiators of signals that are present on the PCB. The predominant cable radiation mechanism appears to be common-mode or "antenna" currents on those cables [4]. It is usually held that the sources of these commonmode cable currents are the high-frequency voltages developed between the ends of the PCB lands [2, 3, 5, 6] to which the cables are attached. These voltages are commonly referred to as "ground drop," although voltage drops across all lands seem to contribute to these currents whether or not the land constitutes a signal return (ground) land. Commonmode currents are also generated on the PCB lands themselves and contribute to direct radiation from the PCB. German experimentally showed a correlation between a reduction in ground drop on a board and a corresponding reduction in the radiated emissions of that board [3]. It should be emphasized that no quantitative relation between ground drop and radiated emissions has been established. However, the experience of this author and others in electromagnetic compatibility (EMC) qualification of typical digital products tends to support the concept that given two printed circuit boards which have identical function and components but different land patterns, the board having the lower levels of ground drop will also have lower levels of radiated emissions. Consequently, the development of a

mathematical model for the prediction of ground drop was deemed to be useful in determining, prior to board construction, which of two candidate land patterns would result in less radiated and conducted emissions.

In addition to radiated and conducted emissions, there are other aspects that affect the functional performance. The digital signals carried by the PCB lands are in the form of trapezoid-shaped current pulses. Rise/fall times of these pulses are of the order of 10 ns. As the digital signals are switched from one state to another, a voltage  $V_{\rm GND}$  is developed across a land inductance which is proportional to the land inductance  $L_{\rm GND}$  and the rate of change of the current through that land, i.e.,

$$V_{\text{GND}}(t) = L_{\text{GND}} \frac{di(t)}{dt}$$
.

For example, a typical PCB land exhibits a land inductance of some 15 nH/in., although this value is dependent on the proximity of nearby lands. Switching of a current of 100 mA in 10 ns in a 5-in. land develops a voltage of 0.75 V across that land. Consequently, the "ground" terminals of two dual in-line packages (DIPs) may be at quite different voltages; this may result in false logic switching, resulting in data-processing errors. As will be shown, the net inductance of the return lands and hence the "ground drop" can be significantly reduced by the close placement of additional return lands. This type of "gridded-ground" system has been shown to be an effective way of reducing ground drop and the associated radiated and conducted emissions [3]. The use of decoupling capacitors is another means for reducing the effect of land inductance [6].

An additional EMI problem that affects the functional performance of a product is crosstalk [7, 8]—the inadvertent coupling of electromagnetic fields from one circuit to another, causing signals in one circuit to appear at the input terminals of devices that are attached to lands of another circuit. These induced signals may degrade the performance of those devices. It will also be shown that closely spaced return lands, as in a gridded-ground system, can significantly reduce the crosstalk.

The primary objective of this paper is to develop a mathematical model for PCBs that can be used to predict the high-frequency voltage drop across PCB lands. Such a model will serve to provide a better understanding of how to arrange land patterns on a PCB in order to reduce voltage drops across the lands, and the resulting conducted and radiated emissions. The prediction of crosstalk, although not the primary purpose of this paper, is a natural by-product of the modeling used. There are numerous models available for the prediction of crosstalk, but none allow the prediction of voltage drop across lands. The modeling described in this paper can be used to predict high-frequency voltage drop as well as crosstalk and is amenable to lumped circuit simulation programs such as ASTAP [9]. The models are an

adaptation of similar notions used in modeling (much smaller) integrated circuits [10–12]. An important objective of this work is to determine the limits of applicability of the model for the much larger PCBs.

Experimental results are given to illustrate the accuracy of the modeling. This experiment will also show that a return land must be placed in very close proximity to its associated signal land in order to significantly reduce the inductance of the return path as well as to reduce crosstalk. A measurement technique that allows the correct measurement of the voltage drop across a land is also described.

### 2. Interpretation of land inductance

There are frequent references to the phrase "inductance of a PCB land" throughout the literature. As indicated previously, it is commonly held that a reduction in the inductances of the lands of a PCB often results in a reduction in the levels of conducted and radiated emissions from that PCB, and there is evidence to support this [3]. But since inductance is conventionally defined for closed loops (because of the requirement for a current), what is meant by the "inductance of a segment of a conductor or portion of a loop?" This notion is often mistakenly thought to mean the frequency-dependent, internal inductance of the conductor due to magnetic flux internal to that conductor. It will be shown that this internal inductance is dominated by an external inductance which is frequency-independent. The following development gives meaning to this notion of the inductance of a segment of a conductor or portion of a loop.

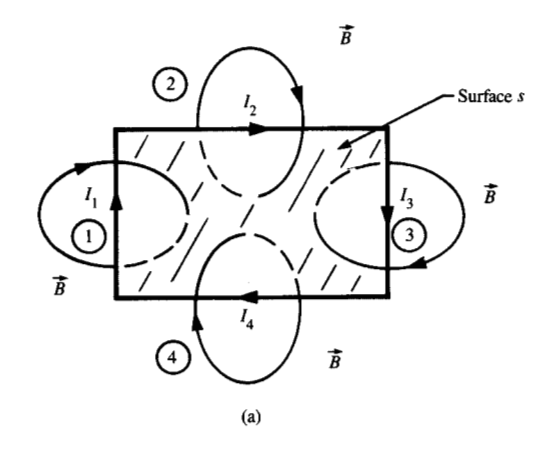
Consider a rectangular loop that supports a current I as shown in Figure 1(a). The currents give rise to a magnetic flux density  $\vec{B}$ . The inductance L of this loop is conventionally defined [13] as the total magnetic flux  $\Psi_m$  penetrating the surface s bounded by the current, viz.,

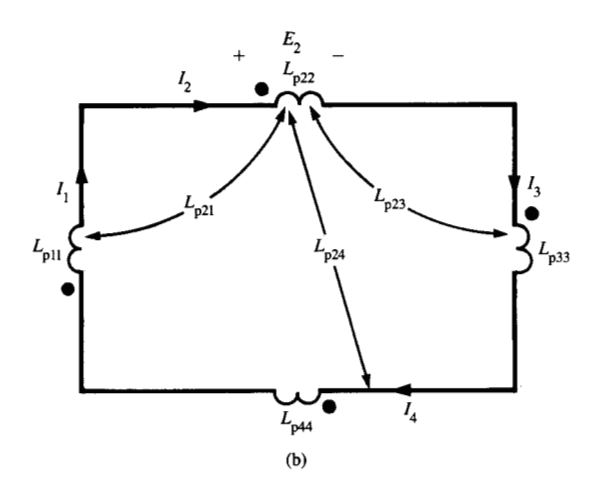
$$\Psi_{\rm m} = \int_{s} \vec{B} \cdot \vec{ds},\tag{1a}$$

per unit of that current, so that

$$L = \frac{\Psi_{\rm m}}{I}.$$
 (1b)

For later purposes we will identify currents associated with individual sides of the rectangle,  $I_i$ , but  $I = I_1 = I_2 = I_3 = I_4$ . We now wish to construct the equivalent circuit of the loop shown in Figure 1(a). The equivalent circuit is depicted in Figure 1(b). Its inductances  $L_{pii}$  are referred to as self partial inductances, and the inductances  $I_{pii}$  with  $i \neq j$  are referred to as mutual partial inductances [14, 15]. These may be defined in a unique and meaningful way by using an alternate form of (1). Since  $\nabla \cdot \vec{B} = 0$ , we may write  $\vec{B}$  in terms of the magnetic vector potential  $\vec{A}$  as  $\vec{B} = \nabla \times \vec{A}$  [13]. Substituting this into (1) and using Stokes' theorem gives [13]





### Figures

Apportioning loop inductance into inductances associated with segments of the loop.

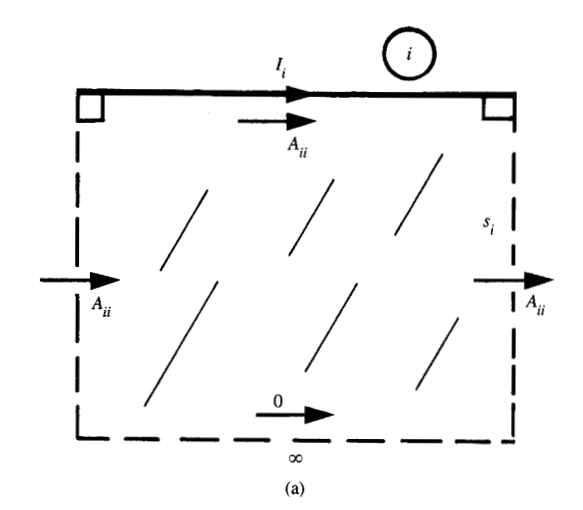
$$L = \frac{\oint_{c} \vec{A} \cdot d\vec{\ell}}{I}, \tag{2}$$

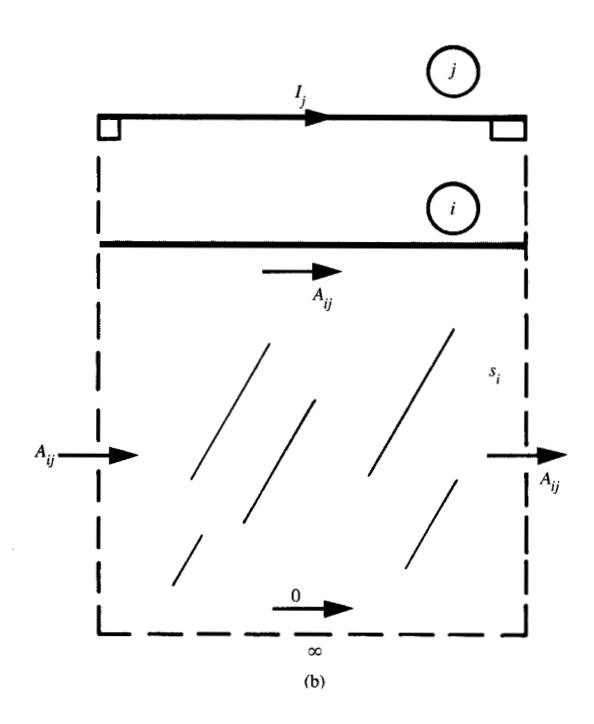
where c is the contour of the loop.

The alternate result in (2) suggests that the partial inductances of the equivalent circuit in Figure 1(b) be defined as

$$L_{\text{pij}} = \frac{\int_{\ell_i} \vec{A}_{ij} \cdot d\vec{\ell}_i}{I_j},\tag{3}$$

where  $\vec{A}_{ij}$  is the magnetic vector potential along segment  $\ell_i$  due to current  $I_j$  on segment  $\ell_j$ . If i = j, these are referred to as self partial inductances, and if  $i \neq j$ , they are referred to as





### E MINITES A

Illustration of the definitions of partial inductance: (a) self partial inductance; (b) mutual partial inductance.

mutual partial inductances. With this definition, the voltage developed across a segment of a conductor can be uniquely and meaningfully obtained. For example, the voltage developed across segment 2 is

$$E_2 = L_{p22} \frac{dI_2}{dt} + L_{p21} \frac{dI_1}{dt} + L_{p23} \frac{dI_3}{dt} + L_{p24} \frac{dI_4}{dt}. \tag{4}$$

We now turn to the important calculation and interpretation of these partial inductances. Ruehli has shown that an alternative to (3) is

$$L_{pij} = \frac{\int_{s_i} \vec{B}_{ij} \cdot d\vec{s}_i}{I_j},\tag{5}$$

where  $s_i$  is the area bounded by the conductor i and infinity and by straight lines that are located at the ends of segment j and are perpendicular to segment j [14]. This is illustrated in Figure 2 for parallel segments. The extension to nonparallel segments is straightforward and is given in [14]. The equivalence between (3) and (5) is important and simple to prove. Utilizing  $\vec{B} = \nabla \times \vec{A}$  and Stokes' theorem, the numerator of (5) can be written as

$$\int_{s_i} \vec{B}_{ij} \cdot d\vec{s}_i = \oint_{c_i} \vec{A}_{ij} \cdot d\vec{\ell}_i, \tag{6}$$

where  $\vec{B}_{ii}$  is the total magnetic flux density penetrating  $s_i$ (which extends from segment i to infinity) and  $\vec{A}_{ij}$  is the corresponding vector magnetic potential associated with  $\vec{B}_{ii}$ along the closed contour  $c_i$  which bounds  $s_i$ . The magnetic vector potential  $\vec{A}$  has two important properties that are crucial to this proof. These are that (1)  $\vec{A}$  is parallel to the current producing it, and (2)  $\vec{A}$  goes to zero as the distance away from the current increases [13]. By construction, the sides of  $s_i$  are perpendicular to segment j, whose current,  $I_i$ , produces  $\vec{A}_{ii}$ . Since  $\vec{A}_{ii}$  is aligned with the current producing it,  $\vec{A}_{ii}$  is perpendicular to the sides of  $s_i$  and as such contributes nothing to the right-hand side of (6) along this portion of  $c_i$ . Also,  $\vec{A}_{ii}$  at infinity is zero, and no contribution is obtained along that part of the contour. Consequently, the only contribution to the right-hand side of (6) is along segment i, as was to be proven. The important result is that the partial inductance  $L_{pij}$  is the ratio of the flux penetrating the surface between segment i and infinity and the current  $I_i$ which produces it. Equivalently,  $L_{pii}$  can also be determined in terms of the vector magnetic potential along segment i, as in (3). Either concept may be used in computing  $L_{pij}$ , but the notion of the relation to magnetic flux through the surface bounded by the segment and infinity is more useful in visualizing qualitative results to be observed in later sections of this paper.

Clearly, the net inductance of a segment of a loop is the sum of the self and mutual partial inductances of that segment, viz.,

$$L_i = \sum_{j=1}^{N} \pm L_{pij},$$
 (7)

where the loop contains a total of N current segments each supporting a current  $I_j$ , and the sign of each term is related to the relative orientation of the currents assigned to segments i and j. Note that for the rectangular loop shown in

Figure 1(a) mutual partial inductances exist only between segments that are not perpendicular to each other, since  $\vec{A}_{ij}$  is perpendicular to segment i for segments j which are orthogonal to segment i. For example,  $L_{p23} = L_{p21} = 0$  and  $L_{p34} = L_{p14} = 0$ . The total loop inductance can then be obtained as

$$L = \sum_{i=1}^{S} L_i, \tag{8}$$

where the loop is broken into S segments. Note that from a knowledge of the self and mutual partial inductances of the loop, the total loop inductance can be determined via (7) and (8), but the reverse is not true; each partial inductance must be computed directly and cannot be determined from a knowledge of L alone.

These notions can also be extended to systems of more than one loop. Each loop can be divided into segments, and the partial inductances due to currents on all segments of all loops can be obtained. Once again, the above notions are meaningful because the voltage drop across a segment can be uniquely determined from Faraday's law and a segmentation of each loop inductance by use of (2). Implicit in these results is the requirement that the electrical dimensions of a portion of the physical system that is represented with these lumped partial inductances be small.

## 3. Determination of lumped circuit elements characterizing PCB land structures

In order to analyze PCB land structures with regard to determining crosstalk and ground drop, lumped circuit elements which characterize those structures must be determined so that lumped circuit analysis programs such as ASTAP [9] may be used to determine the crosstalk and ground drop. This section addresses that problem.

### • PCB land inductance

The previous development implicitly assumes filamentary current segments. Nonuniform current distributions over the conductor cross sections are due to skin effect as well as proximity to nearby conductors [16, 17]. To handle this case, the conductors may be partitioned into subconductors. It is assumed that the current in each subconductor is directed along the subconductor axis and is uniformly distributed over that subconductor cross section. The partial inductances of the subconductors of a conductor can be combined to yield an overall self partial inductance and mutual partial inductances to all other conductors. The technique is essentially the same as combining lumped inductors in parallel and in series into an equivalent lumped inductor. Subconductors of a conductor that are parallel are combined like lumped inductors in parallel, and subconductors that are in series are combined like lumped inductors in series. The technique is described by Ruehli

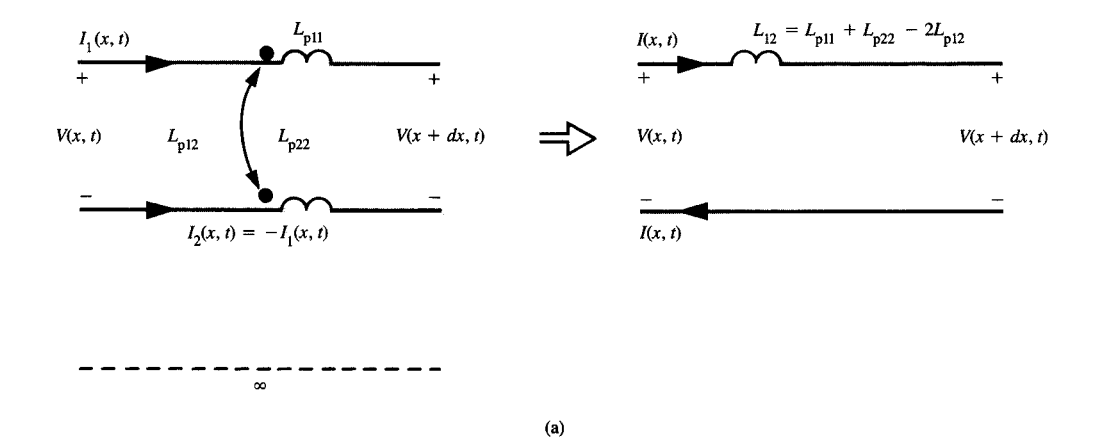
[14]. The result gives self partial inductances,  $L_{\mathrm{p}ii}$ , of all conductors of the system and mutual partial inductances,  $L_{\mathrm{p}ij}$ , between all conductors of the system. A matrixinversion process is used to ensure that all interactions between the subconductors are accounted for. Thus, nonuniform current distributions over the conductor cross sections are effectively taken into account.

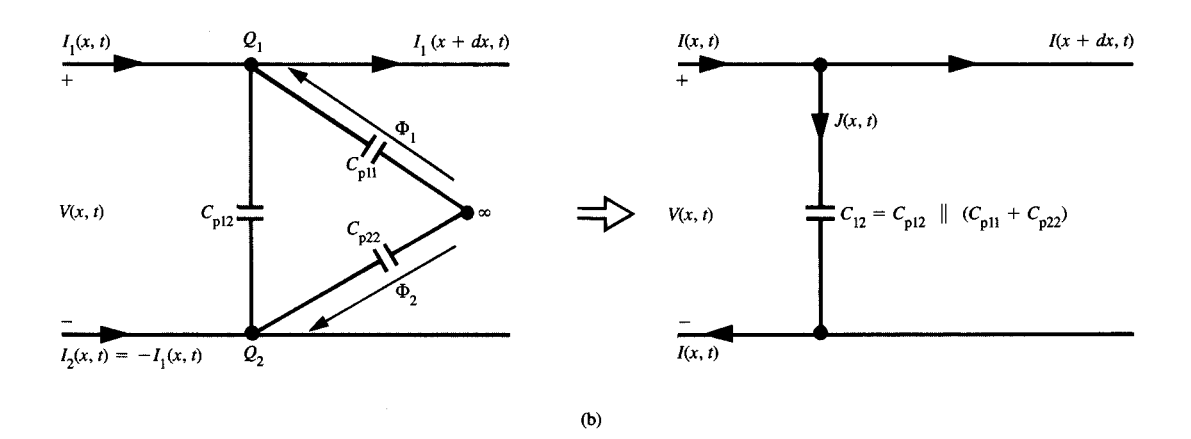
Results for the self and mutual partial inductances for subconductances of rectangular cross section are given by Ruehli [14] and by Hoer and Love [18]. The self and mutual partial inductances of the PCB lands investigated experimentally in this paper are computed using those results according to the above method.

### • Capacitances of PCB lands

A second and equally important parameter in characterizing PCB land structures is the capacitance between its lands. Closed-form expressions for conductors of circular cross section are available [8], but numerical methods must be employed for conductors having rectangular cross sections. Ruehli and Brennan, along with others, have provided numerical methods for calculating these quantities for conductors of rectangular cross section [19]. These methods are in a sense comparable to the method of segmenting conductors into subconductors for the purpose of calculating the partial inductances of the conductors, as described above. The methods take into account nonuniform charge distributions over the conductor surfaces in a fashion dual to the above method for calculation of partial inductances, which takes into account nonuniform distributions of current over the conductor cross sections.

The numerical method for determining the capacitances is essentially comparable to the above method for determining partial inductances. Each conductor face is divided into subfaces, and the charge on each subface is assumed to be uniformly distributed over that subface. There are other possible choices for the charge distribution over the subfaces, but the choice of a uniform distribution simplifies the procedure. The potential of each subface with respect to infinity is related to the charges on each subface with a matrix expression. Each entry can be viewed as a self or mutual partial capacitance of or between subfaces. These partial capacitances associated with the subfaces can be reduced to equivalent self and mutual partial capacitances of the individual conductors in a fashion similar to the reduction of lumped capacitances in parallel or series to an equivalent lumped capacitance. Matrix inversion essentially ensures that interactions between all subfaces are taken into account. The result gives the self partial capacitances of the conductors,  $C_{pii}$ , and the mutual partial capacitances,  $C_{pij}$ , between the conductors. It is important to note that the self partial capacitances  $C_{pii}$  are with respect to infinity rather than directly between conductors, since the potentials used to derive them are with respect to infinity.





Reduction of partial inductances and partial capacitances to (a) loop inductance and (b) capacitance between conductors.

### • Computation of the lumped circuit elements

The equivalent circuit in terms of self and mutual partial inductances for each conductor is sufficient for modeling the inductive effects of the lands. However, it may be further reduced if, instead of choosing n different currents in the conductors, we choose one conductor as the reference through which the other (n-1) currents return, as is done in transmission-line analyses [8]. This is illustrated for a twoconductor line in Figure 3(a). The difference in voltage between the ends of the line for a line of length dx is

$$V(x, t) - V(x + dx, t)$$

$$= L_{p11} \frac{dI_1}{dt} + L_{p12} \frac{dI_2}{dt} - L_{p22} \frac{dI_2}{dt} - L_{p12} \frac{dI_1}{dt}.$$

(9)  $L_{in} = L_{pii} + L_{pnn} - 2L_{pin}$ , (11a)

But  $I_2 = -I_1$ , so that

$$V(x, t) - V(x + dx, t) = (L_{p11} + L_{p22} - 2L_{p12})\frac{dI}{dt},$$
 (10)

where we denote  $I_1 = I$ . Here we identify the "loop inductance" as  $L_{12} = L_{p11} + L_{p22} - 2L_{p12}$ .

For the more general case of a system of n conductors in which the nth conductor is chosen as the reference conductor through which all the other (n-1) currents return, a similar reduction of the partial inductances to loop inductances can be made. The details of such a reduction are given in [14]. The results are

$$L_{ii} = L_{pii} - L_{pin} - L_{pin} + L_{pnn}. {(11b)}$$

For transmission-line analyses, the per-unit-length loop inductances are traditionally employed because the lines are usually assumed to be infinite in length to avoid fringing when computing the line parameters, and partial inductances cannot be defined for lines of infinite length [8]. For the purposes of computing voltages at the endpoints of the line, loop inductances are sufficient. However, loop inductances cannot be used for computing voltages between endpoints of the conductors, since one can only determine the voltages at the endpoints of the line as in (10).

The case of capacitances between conductors is quite similar. Consider the case of two conductors. Recall that the partial capacitances are defined with respect to infinity, as are the partial inductances. The equivalent circuit in terms of partial capacitances is shown in **Figure 3(b)**. In order to reduce this to a lumped capacitance,  $C_{12}$ , between the two conductors, as shown in Figure 3(b), we must eliminate the node at infinity. This is accomplished by noting that the voltage between the conductors can be obtained in terms of the potentials defined with respect to infinity,  $\Phi_1$  and  $\Phi_2$ , as

$$V(x, t) = \Phi_1 - \Phi_2. \tag{12}$$

In addition, the charges of the system of two conductors must satisfy the condition

$$Q_1 + Q_2 = 0 ag{13a}$$

or

$$J_1 + J_2 = 0, (13b)$$

where  $J_i$  is the current into node i. The matrix of partial capacitances relates these quantities as

$$\mathbf{Q} = \mathbf{C}_{\mathbf{p}} \mathbf{\Phi} \tag{14a}$$

or

$$\mathbf{J} = \mathbf{C}_{p} \frac{d}{dt} \mathbf{\Phi}. \tag{14b}$$

The entries in  $C_{\scriptscriptstyle D}$  are composed of the partial capacitances:

$$\mathbf{C}_{p} = \begin{bmatrix} C_{p11} + C_{p12} & -C_{p12} \\ -C_{p12} & C_{p22} + C_{p12} \end{bmatrix}. \tag{15}$$

These constraints can be imposed if we invert (14) to yield, for this two-conductor system,

$$\frac{d}{dt} \begin{bmatrix} \Phi_1 \\ \Phi_2 \end{bmatrix} = \frac{1}{\Delta} \begin{bmatrix} C_{p22} + C_{p12} & C_{p12} \\ C_{p12} & C_{p11} + C_{p12} \end{bmatrix} \begin{bmatrix} J_1 \\ J_2 \end{bmatrix}, \tag{16a}$$

where

$$\Delta = C_{\text{pl1}}C_{\text{p22}} + C_{\text{pl1}}C_{\text{pl2}} + C_{\text{p22}}C_{\text{pl2}}.$$
 (16b)

Subtracting the second row of (16a) from the first yields, according to (12),

$$\frac{d}{dt} V(x, t) = \frac{1}{\Delta} \left[ C_{p22} - C_{p11} \right] \begin{bmatrix} J_1 \\ J_2 \end{bmatrix}. \tag{17}$$

Imposing (13b) and defining

$$I(x + dx, t) - I(x, t) = J(x, t)$$
 (18)

vields

$$\frac{d}{dt}V(x,t) = \frac{C_{p11} + C_{p22}}{\Delta}[I(x,t) - I(x+dx,t)].$$
 (19)

Inverting (19) yields the capacitance between the two conductors as

$$C_{12} = \frac{\Delta}{C_{p11} + C_{p22}}$$

$$= C_{p12} + \frac{C_{p11}C_{p22}}{C_{p11} + C_{p22}}$$

$$= C_{p12} \| (C_{p11} + C_{p22}), \tag{20}$$

where || denotes "in parallel with" and where we treat the capacitor impedances as resistors.

For the general case of an n-conductor system, the partial capacitances defined with respect to infinity can be reduced similarly to capacitances between pairs of conductors,  $C_{ij}$ . The details are described in [20, 21]. The result is

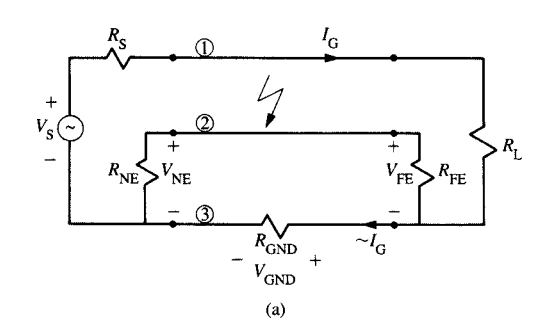
$$C_{ij} = C_{pij} + \frac{C_{pii}C_{pjj}}{\sum_{k=1}^{n} C_{pkk}}.$$
(21)

In the analyses to be presented in this paper, a mixture of the above characterizations will be used to define the lumped circuit characterizing the land structures. The partial inductances will be used instead of loop inductances, since we are interested in determining the voltage drops across the lands (ground drop) as well as the voltages at the ends of the lands (crosstalk). However, the conductor-to-conductor capacitances will be used rather than the partial capacitances because the node at infinity constitutes an unnecessary complication.

### • Land resistance

For conductors of circular cross section (wires), it is well known that high-frequency currents are concentrated near the outer periphery of the conductors [22]. This is referred to as skin effect and results in the conductors having a frequency-dependent impedance in addition to the net partial inductance of that conductor. The conductor resistance remains at the dc value up to a point where the wire radius is of the order of a skin depth. Above that frequency the resistance, R(f), increases as the square root of the frequency. Similarly, the inductance of the wire due to magnetic flux internal to the wire,  $L_i$ , remains at the dc level of  $5 \times 10^{-7}$  H/m up to this point and decreases as the square root of frequency above that frequency. This is referred to as internal inductance,  $L_i$ , and its inductive reactance,  $\omega L_i$ , therefore increases as  $\sqrt{f}$ . The net impedance of the wire is





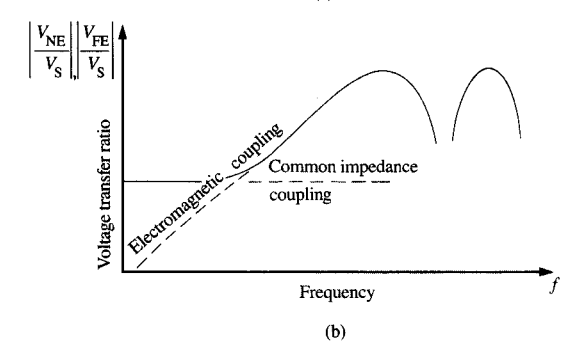


### Figure (

Illustration of common impedance coupling and its effect on the frequency response of crosstalk.

the sum of these internal impedances and the net partial inductive reactance of the wire,  $L_p$ , as

$$Z(f) = R(f) + j\omega [L_{i}(f) + L_{n}].$$
 (22)

For conductors having rectangular cross sections, few such quantitative results are known, although there is little doubt that the qualitative aspects of the phenomenon are very similar to the case of conductors having circular cross section [16, 17, 23]. For most cases of interest, the partial inductance dominates the internal inductance. If this is true at dc, it is certainly true for higher frequencies, since the internal inductance decreases as  $\sqrt{f}$ . For most practical cases, then, the internal inductances of the lands may be neglected, as is done in this paper.

Although the frequency dependence of the skin-effect resistance, R(f), is well-characterized for sinusoidal excitation, its usage in time-domain calculations is complicated [23]. For the results shown in this paper, it is shown that the inductive reactance of the net partial inductance of the conductor,  $\omega L_{\rm p}$ , dominates the resistance term when skin effect becomes well-developed and where R(f) deviates from its value at dc,  $R_{\rm dc}$ . Therefore, we shall approximate R(f) as its dc value.

This dc resistance is also shown to be important at low frequencies. This effect is illustrated in **Figure 4**. The magnitudes of the near-end and far-end crosstalk voltages for a three-conductor line are shown as voltage transfer ratios. It can be shown that for lines composed of perfect conductors, the crosstalk increases linearly with frequency by 20 dB per decade for resistive loads [24]. At lower frequencies there is an additional and dominant component of that crosstalk which is due to imperfect conductors and is frequently referred to as "common-impedance coupling." This is quite simple to see. For a sufficiently small frequency, the current in the driven or generator line,  $I_{\rm G}$ , is approximately determined as

$$I_{\rm G} = \frac{V_{\rm S}}{R_{\rm S} + R_{\rm I}},\tag{23}$$

since  $R_{\rm GND}$  is small compared to  $R_{\rm S}$  and  $R_{\rm L}$ . The majority of this current passes through the common return conductor, developing a voltage drop of

$$V_{\rm GND} = R_{\rm GND} I_{\rm G} \tag{24}$$

across that conductor. This voltage is divided across the near end and far end of the pickup or receptor circuit to yield

$$\frac{V_{\rm NE}}{V_{\rm S}} = \frac{R_{\rm NE}}{R_{\rm NE} + R_{\rm FE}} \frac{R_{\rm GND}}{R_{\rm S} + R_{\rm L}},$$
 (25a)

$$\frac{V_{\rm FE}}{V_{\rm S}} = -\frac{R_{\rm FE}}{R_{\rm NF} + R_{\rm FE}} \frac{R_{\rm GND}}{R_{\rm S} + R_{\rm L}},$$
 (25b)

which is frequency-independent. This provides a "floor" for the total crosstalk and is clearly seen in the experimental results to be presented. As will be seen, if one is only interested in the frequency range of the FCC regulatory limits (450 kHz to 1 GHz), the land resistances can be removed from the model for typical board dimensions. On the other hand, if one is interested in calculating the functional performance of the board, the land resistances cannot be omitted, since a significant portion of the spectral content of the signals may lie in the lower-frequency components.

### 4. Circuit characterization of the lands

There are numerous ways to model the PCB land structures by arranging the lumped elements that were developed previously. If the lands are parallel and have uniform cross sections along their length, and if their length-to-width separation ratio is large, a distributed-parameter transmission-line model can be used [8]. The resistive, inductive, and capacitive elements in this model are perunit-length values and may be approximately obtained from the previous results by dividing those total elements by the length of the line. For sinusoidal excitation, the transmission-line equations are derived in the conventional manner, resulting in [8]

$$\frac{d}{dx}\mathbf{V}(x) = -[\mathbf{r}(f) + j\omega\mathbf{l}]\mathbf{I}(x), \tag{26a}$$

$$\frac{d}{dx}\mathbf{I}(x) = -j\omega\mathbf{c}\mathbf{V}(x),\tag{26b}$$

where the line axis is denoted as x. The (n-1)-dimensional vectors  $\mathbf{V}(x)$  and  $\mathbf{I}(x)$  contain the line phasor voltages (with respect to the reference conductor) and currents, respectively, and the  $(n-1)\times (n-1)$  matrices  $\mathbf{r}$ ,  $\mathbf{l}$ , and  $\mathbf{c}$  contain the per-unit-length line parameters. Computer programs have been written to solve those differential equations for sinusoidal excitation and incorporate the terminal constraints [25]. In addition to its inability to predict voltage drop across the line conductors, there is an additional difficulty associated with this transmission-line model; conventional lumped circuit programs cannot be used to solve these equations. In addition, the direct, time-domain solution of the transmission-line equations is difficult.

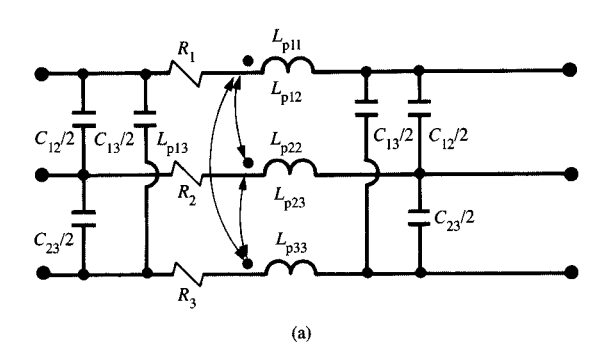
More common ways of modeling these lines are with lumped circuit iterative structures [8]. Two examples are shown in Figure 5 for a three-conductor line. These are referred to as the Lumped Pi and the Lumped Tee structures because of their physical appearance. The Lumped Pi structure is used to characterize the PCB land structures in the computed results to be shown, and the ASTAP circuit analysis program is used to solve the resulting lumped-element circuit for the prediction of crosstalk and ground drop (across the reference conductor, which is conductor 3 in Figures 4 and 5).

Crosstalk predictions are obtained with both the transmission-line model and the Lumped Pi model. In the transmission-line model, the per-unit-length loop inductance matrix, l, in (26a) is computed from capacitance calculations as [8]

$$\mathbf{I} = \frac{1}{v_0^2} \, \mathbf{c}_0^{-1},\tag{27}$$

where  $c_0$  is the  $(n-1)\times (n-1)$  per-unit-length capacitance matrix with the surrounding dielectric (the PCB) removed, and  $v_0$  is the speed of light in air. This is a "high-frequency inductance" in that it presumes that skin effect is well-developed and that currents are confined to the conductor surfaces [14]. Assuming the current to be uniformly distributed over the conductor cross section would give de inductances. For conductors that are widely spaced, there is usually very little difference between these two [10, 14]. By using the numerical techniques outlined in the subsections on capacitances of PCB lands and computation of lumped circuit elements, both  $c_0$  and c are computed by dividing those capacitances computed for a line of total length  $\mathcal L$  by that line length; i.e.,

$$\mathbf{c}_0 = (1/\mathcal{L}) \mathbf{C}_0$$
 and  $\mathbf{c} = (1/\mathcal{L})\mathbf{C}$ .



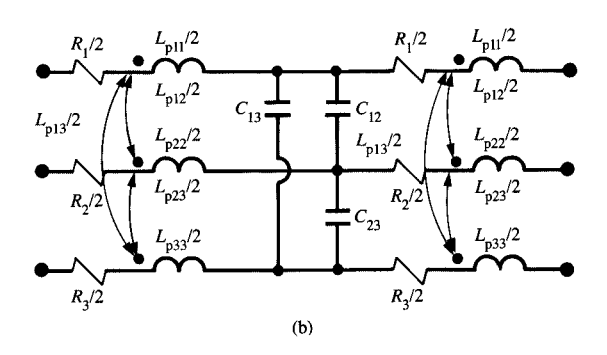


### Figure .

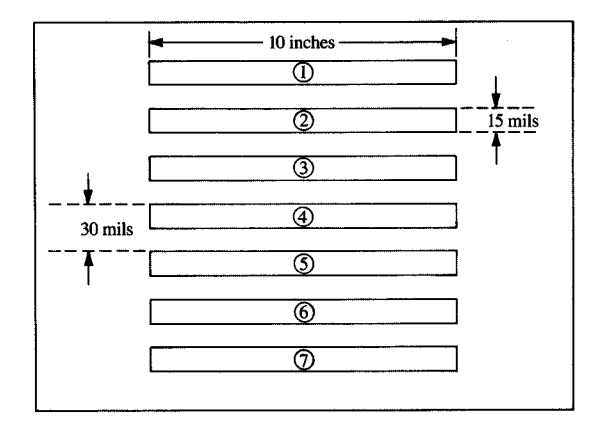
Lumped circuit models: (a) lumped Pi and (b) lumped Tee

It should be pointed out once again that voltage drop across the line conductors cannot be predicted with the transmission-line model, since loop inductances are used in that model. Loop inductances could also be used in the Lumped Pi model once a conductor is designated as reference, but we use partial inductances computed by the numerical methods of the subsection on PCB land inductance in the Lumped Pi model so that the voltage drop across the return conductor can be predicted.

Land patterns on PCBs are predominantly in the form of chains of rectangular conductors whose widths vary along the chain. These types of patterns can be modeled using the previously described techniques by breaking the conductors into individual lengths of uniform cross section. Each conductor subsection can then be modeled as described previously, and the conductors can then be reconnected in the model.

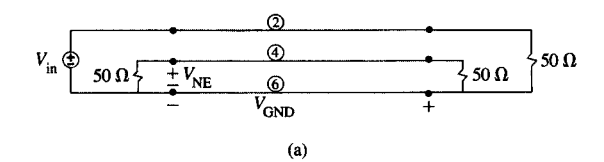
# 5. Comparison of model predictions and experimental results

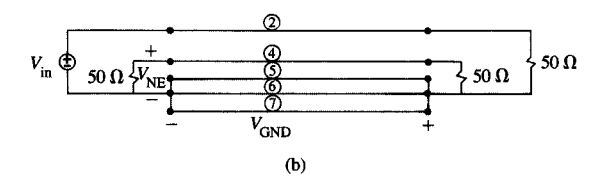
Four configurations were measured. They were formed from a set of seven parallel lands 10 inches in length. The land

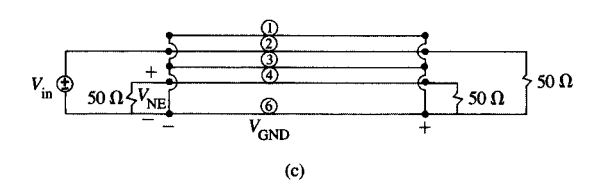


### Figure 6

Experimental land pattern.







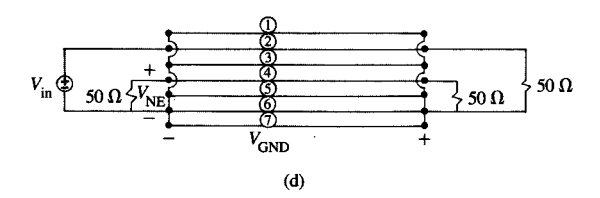


### Figure 7

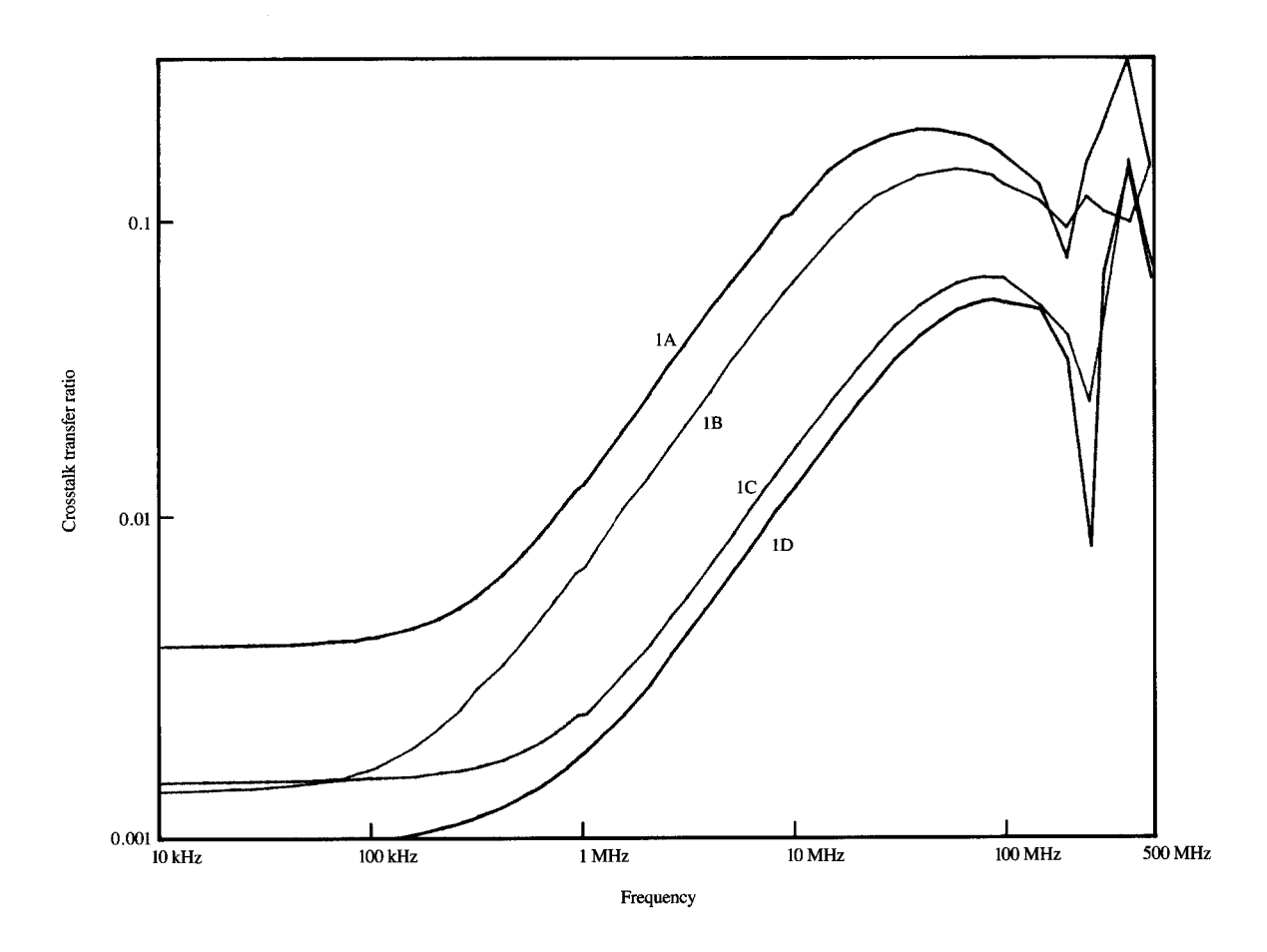
The four configurations that were investigated, numbered in accordance with pattern shown in Figure 6: (a) configuration 1A; (b) configuration 1B; (c) configuration 1C; (d) configuration 1D.

thicknesses were 1.38 mils, corresponding to one-ounce copper cladding. The supporting board was glass-epoxy  $(\epsilon_r = 4.7)$  having a thickness of 47 mils. The basic land pattern used is shown in Figure 6. The land widths were 15 mils, and the center-to-center land separations were 30 mils. The four configurations formed from the basic pattern are illustrated in Figure 7. The lands are numbered with reference to Figure 6. Load resistances of 50  $\Omega$  were used. and land 2 with respect to land 6 was driven at the left end with a zero source impedance sinusoidal source,  $V_{\rm in}$ , and terminated at the far end in 50  $\Omega$ . Lands 4 and 6 were also terminated at each end in 50  $\Omega$ . The remaining lands (1, 3, 5, 7) were either removed or connected in parallel with the reference land (no. 6) to illustrate the effect of placement of additional ground lands. The frequency response of the crosstalk at the near end,  $V_{\rm NE}$ , was measured, and the magnitude of the crosstalk transfer ratio,  $V_{\rm NE}/V_{\rm in}$ , will be shown. Also, the frequency response of the magnitude of the ground drop transfer ratio,  $V_{GND}/V_{in}$ , will be shown. The phase of these transfer ratios was also measured but will not be shown. The frequency response of these quantities is of primary interest because the FCC limits are stated in the frequency domain.

The measurements were made at frequencies of 1, 1.5, 2, 2.5, 3, 4, 5, 6, 7, 8, and 9 in each decade from 10 kHz to 500 MHz. Hewlett-Packard 3400A RMS voltmeters were used to monitor  $V_{\rm in}$ ,  $V_{\rm NE}$ , and  $V_{\rm GND}$  from 10 kHz to 1 MHz. A Hewlett-Packard 8405A Vector Voltmeter was used to measure these quantities from 1 MHz to 500 MHz.

The four configurations were chosen to illustrate the importance of the judicious placement of ground lands on a PCB. Configuration 1A contained only one ground (signal return) land. Configuration 1B contained two additional ground lands, as did configuration 1C. The two additional ground lands of configuration 1B were not placed as close to the driven conductor as they were in configuration 1C. Configuration 1D contained four additional ground lands and was a combination of 1B and 1C. Note that the lands were quite close to each other in all four configurations. However, we will find that in order to achieve a significant reduction in both crosstalk and ground drop, the ground lands must be placed very close to driven land. For example, the crosstalk and ground drop of configuration 1B were some 5 dB below those of 1A, but the crosstalk and ground drop of configuration 1C were some 16 dB below those of 1A! Going to the pattern of configuration 1D provided only some 3 dB additional reduction from that of 1C. Hence, ground lands must be placed very close to the driven land in order to significantly reduce crosstalk and ground drop.

The predictions of crosstalk were obtained with both the transmission-line model and the Lumped Pi model, whereas the predictions of ground drop were obtained from the Lumped Pi model. The land inductances and capacitances used in these models were obtained as described above. In computing the partial inductances, each land was partitioned



Comparison of measured crosstalk transfer ratio for the four experimental configurations.

into 15 subconductors by using five partitions across the width and three partitions across the thickness. In computing the partial capacitances, the width was partitioned into five divisions, the thickness into one division, and the length into seven divisions, giving a total of 84 subfaces for each land.

### • Crosstalk

The experimentally obtained crosstalk transfer ratios are compared in **Figure 8**. Compare these to Figure 4. From 10 kHz to 100 kHz, these are frequency-independent, which is due primarily to common impedance coupling, as described previously. Because configurations 1B and 1C contain three ground lands in parallel, their levels should be 1/3 of the level for 1A. In fact, the ratios at 10 kHz are 2.94 and 3.15, respectively. Similarly, 1D contains five ground lands in parallel. The ratio of the level for configurations 1A and 1D at 10 kHz is 4.94. From 1 MHz to 10 MHz the levels increase at a rate of 20 dB per decade, as explained

previously. Above 100 MHz, we observe the usual rapid variation with frequency, since the line is electrically long in this frequency range. Using numerical methods, the effective dielectric constant  $\epsilon_r = C/C_0$  was computed for a two-land line to be 2.62. Thus, the 10-in. line was one wavelength ( $\lambda$ ) long at 730 MHz. Therefore, the line was  $\lambda/5$  at 146 MHz. Thus, the range of frequencies above 150 MHz may be considered to constitute the range for which the line is electrically long. Modeling the entire line with only one Lumped Pi model would not be expected to give accurate predictions above, for example, 150 MHz. For frequencies above 150 MHz, the conductors must be divided into segments of smaller length, and Lumped Pi models must be constructed for them. This results in a larger lumped circuit to be solved, although codes such as ASTAP would be able to solve these larger circuits.

The predictions of the transmission-line model and the Lumped Pi model (labeled as ASTAP) are shown for



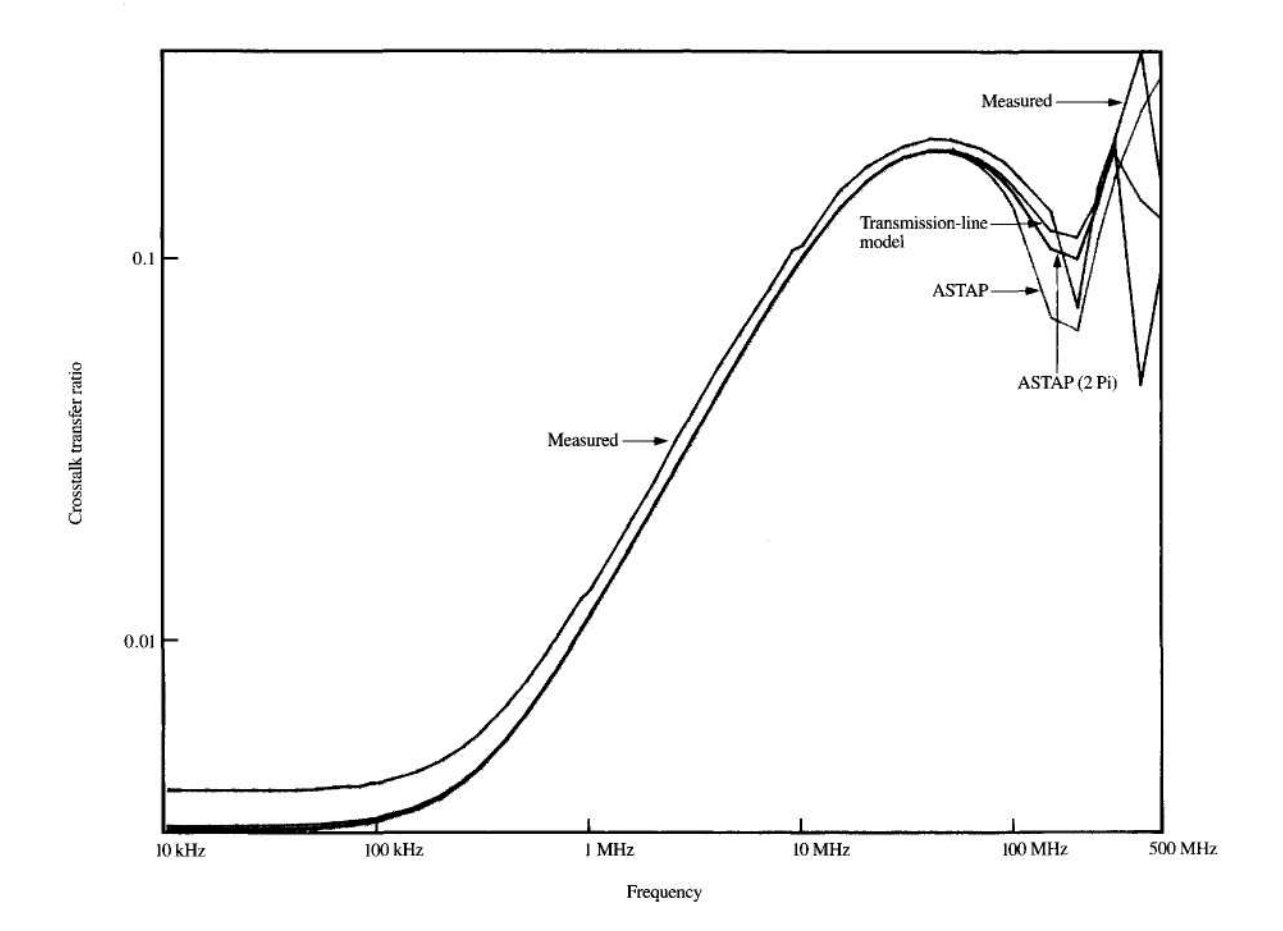


Figure 9

Predicted compared to measured crosstalk transfer ratio for configuration 1A.

configuration 1A in Figure 9. The model gives similar prediction accuracies for the other configurations. Predictions below 100 MHz are within 3 dB of the experimental data. Predictions of the Lumped Pi model using two Pi sections for the entire line are also shown for 1A in Figure 9 [ASTAP (2 Pi)]. Note that at 10 kHz the models underpredict the "common-impedance coupling level." This level is directly related to the land impedance, as shown by (25), and should be easy to predict. The dc land resistance was calculated directly from the assumed land cross-sectional dimensions (15 mils × 1.38 mils). Because levels at 10 kHz are not well predicted, the only source of error should be the land dimensions and/or the conductivity of the land material. Investigation of the land widths with a microscope revealed that their widths were approximately 15 mils. The assumption of copper having a conductivity of 5.8  $\times$  10<sup>7</sup> S/m as the cladding material is probably also valid, so

the only other source of this error is in the assumed land thickness. One can compute from (25) and the measured levels at 10 kHz that a land thickness of 1.1 mils yields a correct prediction of the common-impedance coupling level. Discussions with the board manufacturer indicated that this 25% reduction in cladding thickness from the nominal value of 1.38 mils would not be unreasonable to expect.

The prediction of the time-domain (transient) crosstalk was also investigated. A Hewlett-Packard 8082A pulse generator was set to provide an open-circuit trapezoidal pulse voltage waveform of 1-V peak with 20-ns rise/fall times and a repetition rate of 1 MHz with a 50% duty cycle. The pulse generator was attached to the inputs of the four configurations, and the time-domain near-end crosstalk was measured with a Tektronix 7834 400-MHz oscilloscope. A comparison of the peak levels with those predicted with the Lumped Pi model and ASTAP is given in **Table 1**. The

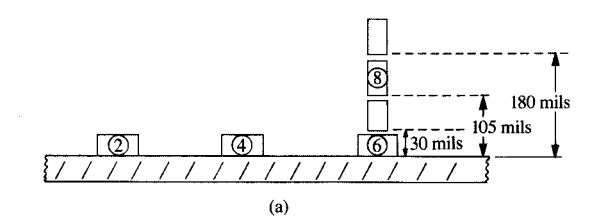
predicted waveshapes were virtually identical in form to those measured. The time-domain ground drop was similarly measured and computed. Prediction accuracies similar to those for the time-domain crosstalk were observed.

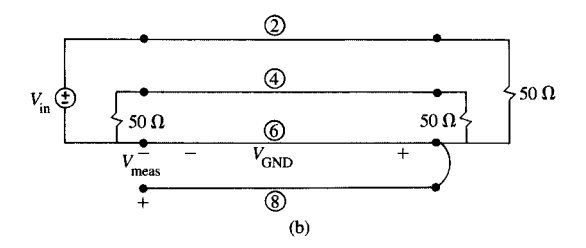
As is evident from Figure 9, the lumped circuit models shown in Figure 5 are valid so long as the structure they are used to represent is electrically small. For time-domain predictions, this means that spectral components of the timedomain signals below a certain frequency will be wellpredicted, whereas spectral components above that frequency will be poorly predicted. Thus, lumped circuit models have difficulty predicting certain high-frequency properties of the waveform such as rise/fall times. This pulse spectrum consists of discrete-frequency components at multiples of 1 MHz. A bound on these spectral amplitudes consists of a 0-dB-per-decade level up to 637 kHz, a -20-dBper-decade level up to 16 MHz, and a -40-dB-per-decade level above that [7]. These results indicate that errors in predicting the high-frequency spectral components are not significant in the prediction of the time-domain pulse waveshape and level so long as the pulse rise/fall times are sufficiently greater than the one-way transit time of the board, which in this case is of the order of 1.4 ns [7].

### • Ground drop

The experimental measurement of ground drop is much more difficult than measurement of crosstalk since it is required that the voltage be measured between two widely spaced points (the two ends of the ground lands). The initial measurement used a small, insulated wire lying on top of the ground land and soldered at the far end to the ground land. The voltage between the near end of this wire and the near end of the ground land was measured. This measurement configuration was chosen in order to minimize the loop area between the measurement wire and ground land so as to minimize any extraneous voltages induced in this loop caused by magnetic fields of the currents in the system. However, it will be shown that this is perhaps the worst possible placement of the measurement wire; it should be placed as far as possible from the ground land in order to measure the ground drop accurately. This point was noted by Skilling [26], who gave an alternative rationale for its

To illustrate this point, a measurement conductor was placed parallel to and at different heights above the ground land for configuration 1A, as shown in Figure 10(a), by placing a similar PCB on edge along the ground land. A schematic of the configuration is shown in Figure 10(b). The measured voltages,  $V_{\rm meas}$ , are plotted in Figure 11 for various heights of the measurement land. Note that all measured levels from 10 kHz to 100 kHz are virtually identical, as they should be since these are directly related to  $R_{\rm GND}$  [see Figure 4 and Equation (25)]. However, at frequencies from 1 MHz to 100 MHz, the measured levels increase for increased





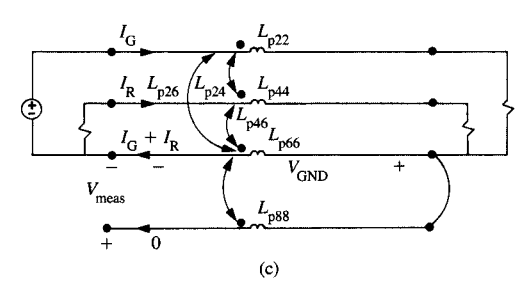


# Figure 10 Measurement of ground drop: (a) physical configuration, (b) schematic, and (c) inductance model using partial inductances.

 Table 1
 Peak time-domain near-end crosstalk.

| Configuration | Measured<br>(mV) | Predicted (mV) |
|---------------|------------------|----------------|
| 1A            | 42               | 38.1           |
| 1 B           | 24               | 19             |
| 1C            | 6.5              | 4.7            |
| 1D            | 4.5              | 3.27           |

height of the measurement conductor and converge. One might expect that the additional voltage drops around the measurement loop (consisting of lands 6 and 8) due to the magnetic flux through this loop would cause the measured voltage,  $V_{\rm meas}$ , to differ from the desired ground drop voltage  $V_{\rm GND}$ . The following results show that, in fact, the reverse is true;  $V_{\rm meas}$  approaches  $V_{\rm GND}$  for increasing height of the measurement conductor!

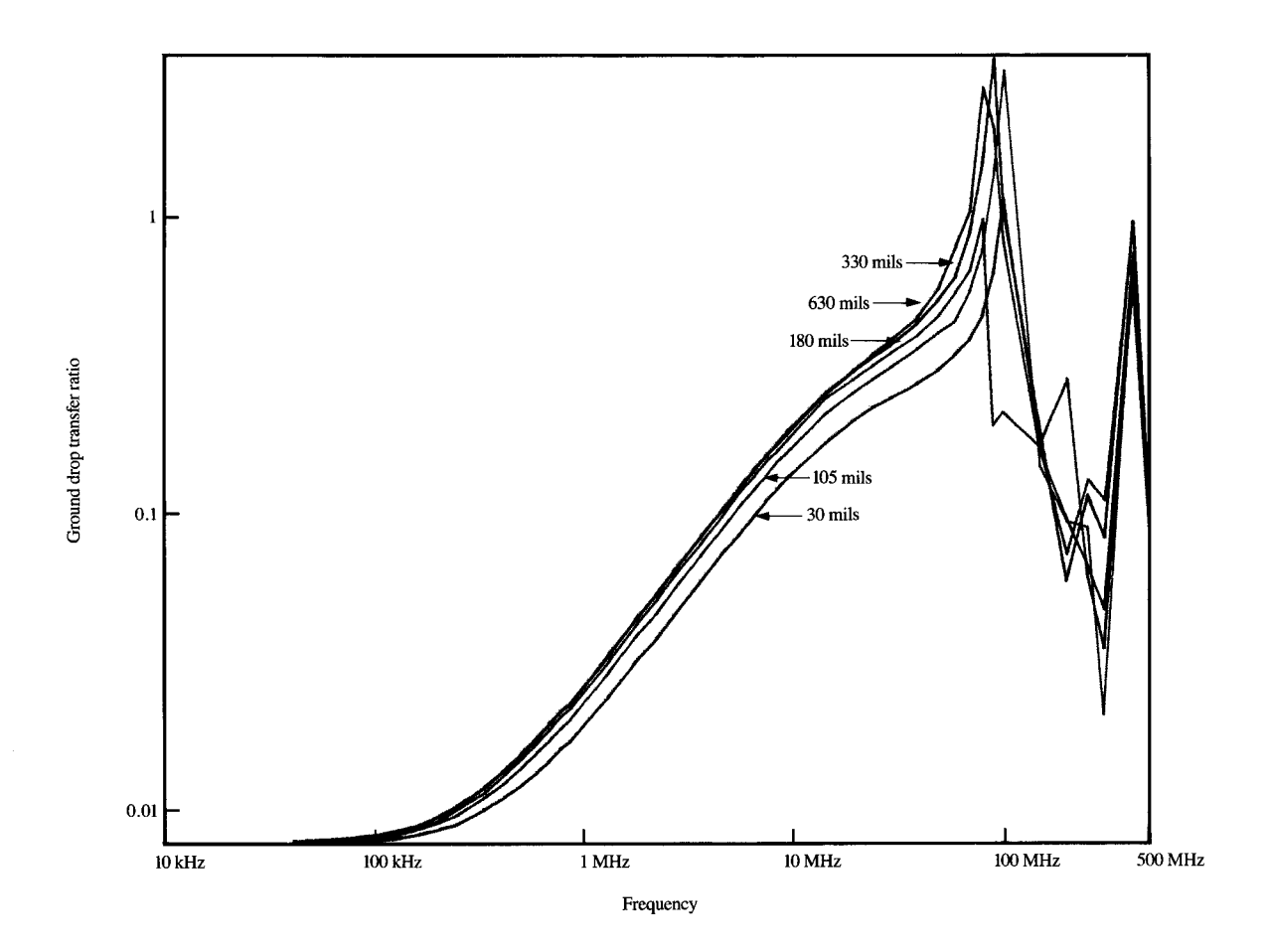


Figure 11

Comparison of measured ground drop transfer ratio for configuration 1A for various heights of land.

This result can be readily explained with an understanding of the meaning of partial inductances developed in Section 2. Consider the inductive equivalent circuit shown in Figure 10(c). Note that these are partial inductances and not loop inductances. The voltage  $V_{\rm meas}$  was measured with a high-impedance voltmeter, so it is reasonable to assume zero current through the measurement conductor. It is also reasonable to assume that the generator and receptor circuit currents,  $I_{\rm G}$  and  $I_{\rm R}$ , respectively, return through the ground land. From that circuit, the difference between  $V_{\rm meas}$  and  $V_{\rm GND}$  is the voltage drop across the self partial inductance of the measurement conductor,  $L_{\rm p88}$ , viz.,

$$V_{\text{meas}} - V_{\text{GND}} = L_{\text{p28}}I_G + L_{\text{p48}}I_R - L_{\text{p68}}(I_G + I_R)$$
$$= (L_{\text{p28}} - L_{\text{p68}})I_G + (L_{\text{p48}} - L_{\text{p68}})I_R.$$
(28)

We desire

$$V_{\text{meas}} = V_{\text{GND}}, \tag{29}$$

which will be true only if  $L_{\rm p28}=L_{\rm p68}$  and  $L_{\rm p48}=L_{\rm p68}$ . Recall that these mutual partial inductances are the ratio of the flux between one conductor and infinity and the current in the other conductor. Observing Figure 10(a), we see that as we move the measurement conductor (no. 8) higher above the ground conductor,  $L_{\rm p28} \rightarrow L_{\rm p68} \rightarrow L_{\rm p48}$ , and (28) reduces to (29)! Thus, an understanding of partial inductances is the key to accurate measurement of ground drop.

The experimentally measured ground drops are shown for configurations 1A, 1B, 1C, and 1D in Figure 12 at the largest height, 630 mils. Note that the different ground land placements show a reduction in ground drop similar in magnitude to the reductions in crosstalk shown in Figure 8. Once again, ground lands must be placed extremely close to the driven land to achieve any significant reduction in ground drop!

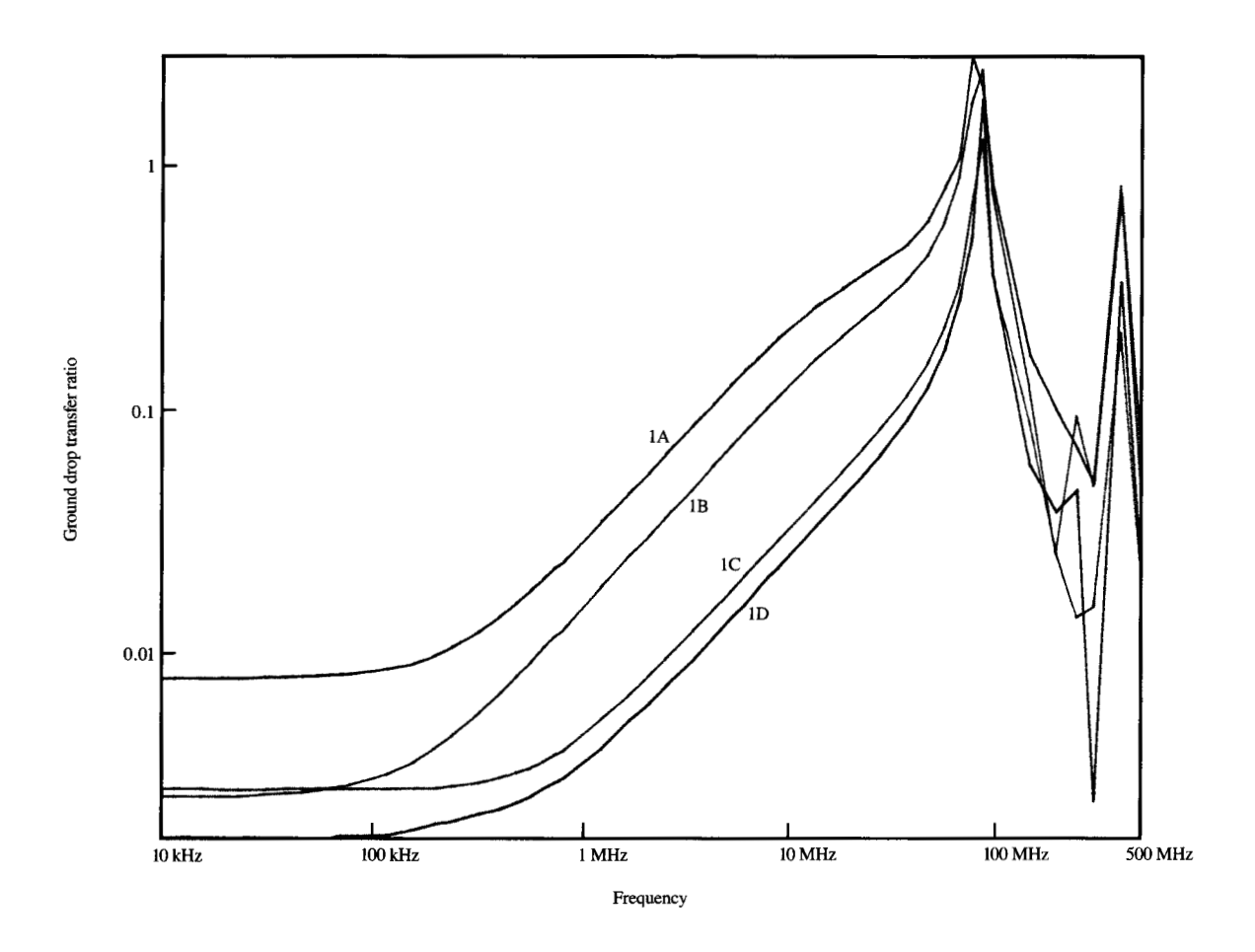


Figure 12

Comparison of measured ground drop transfer ratio for the four experimental configurations for a land height of 630 mils.

The predictions of  $V_{\rm GND}$  with the Lumped Pi model (ASTAP) are shown for configuration 1A in Figure 13. These are quite accurate below some 50 MHz for the maximum height of the measurement conductor (630 mils). Predictions of  $V_{\rm GND}$  for the other land configurations show a similar accuracy. This tends to confirm that  $V_{\rm meas}$  converges to  $V_{\rm GND}$  as the height of the measurement conductor above the ground land increases. With a correct value of  $R_{\rm GND}$ , the predictions should converge to the measured value at 10 kHz.

Note that for all the configurations, the measured ground drop shows a peak at around 80 MHz. This peak in  $V_{\rm meas}$  is not truly a part of  $V_{\rm GND}$  but is due to the presence of the measurement land (no. 8) and the loading of the vector voltmeter used to measure  $V_{\rm meas}$ . To confirm this, the inductances and capacitances were recomputed for configuration 1A to include the measurement conductor (no.

8) and were included in the Lumped Pi model. The loading of the vector voltmeter was included as a resistance (100 k $\Omega$ ) in parallel with a capacitance (2.5 pF plus 5 pF of probe capacitance) between the near ends of lands no. 6 and no. 8 (across  $V_{\rm meas}$ ). The measured voltage,  $V_{\rm meas}$ , was computed from this model, and the results are also shown in Figure 13. Note that including (1) the measurement land and (2) the loading of the measurement voltmeter allows a very accurate prediction of the peak at 80 MHz. In fact, the predictions are quite good up to 150 MHz.

Evidently, the inductance of the measurement loop formed by lands no. 6 and no. 8 combined with the capacitance of the measurement voltmeter caused this resonance at 80 MHz. This illustrates a practical limit on the height to which one may raise the measurement conductor above the ground land. Increasing this height increases the inductance of the measurement loop, which causes the



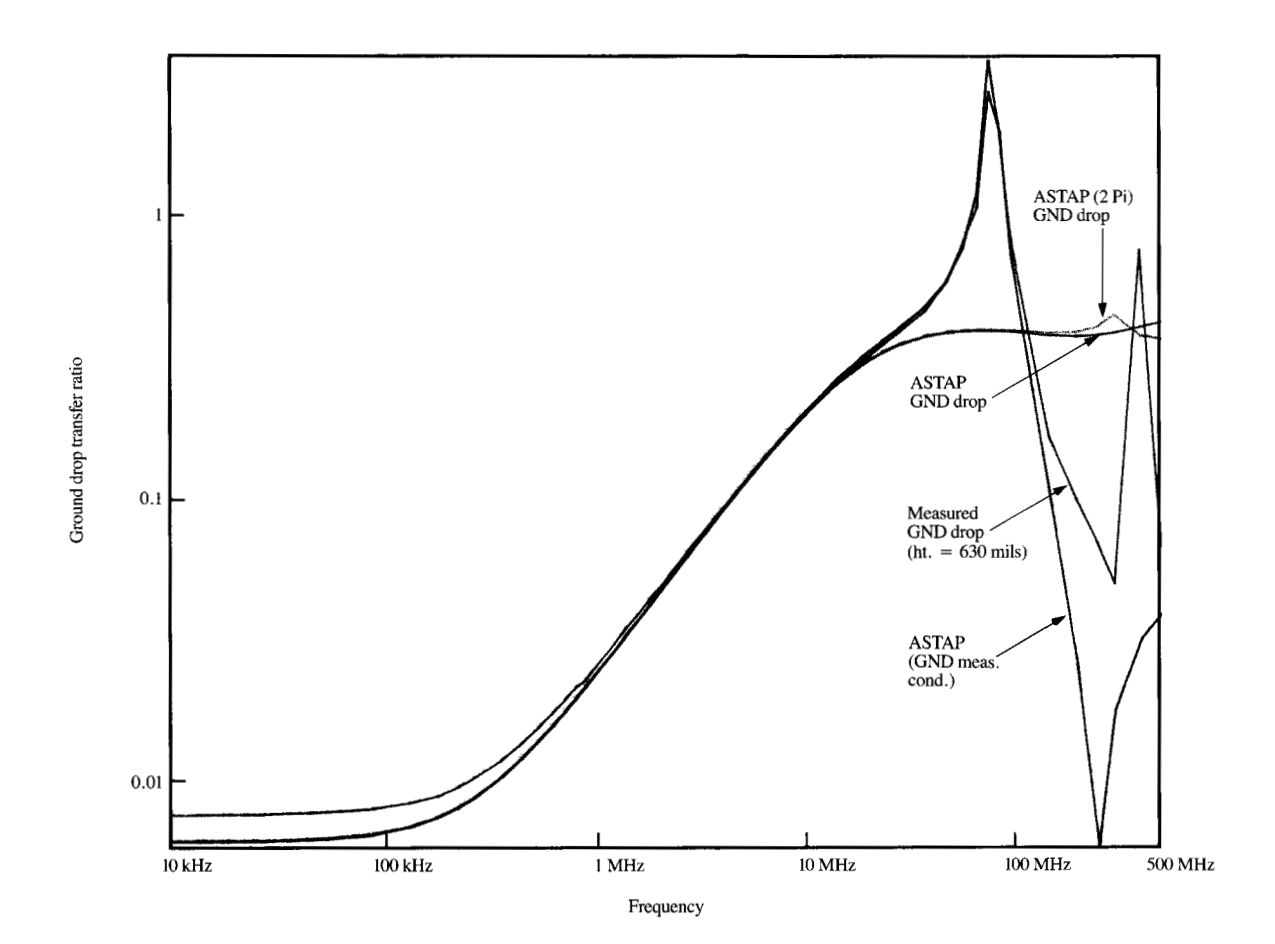


Figure 13

Predicted compared to measured ground drop transfer ratio for configuration 1A.

resonance to occur at lower frequencies. This point is evident in Figure 11, which shows the results for configuration 1A for increasing heights of the measurement conductor.

### 6. Summary and conclusions

The modeling and prediction of crosstalk and ground drop on PCBs has been investigated. For typical PCB land dimensions one should be able to predict crosstalk for frequencies of 100–200 MHz. Use of a distributed-parameter transmission-line model or more sections of the Lumped Pi or Tee models extends this prediction range.

The accurate prediction and measurement of voltage between the two ends of the signal return land (ground drop) required the use and understanding of the concepts of partial inductance. A transmission-line model is inherently incapable of predicting ground drop because that model uses loop inductances. Partial inductances used in a lumped circuit model allow the accurate prediction of ground drop up to frequencies for which the line lengths are of the order of  $\lambda/5$ . For typical board dimensions one should be able to predict ground drop up to frequencies of 100–200 MHz. A finer segmentation of the conductors along their largest dimension (length) and the subsequent use of more Lumped Pi or Tee sections should extend that frequency range.

The correct measurement of ground drop could be explained in terms of the concept of partial inductance. It appears that accurate measurement of ground drop requires that the measurement conductor be placed far from the ground land. However, resonances caused by the inductance of the measurement loop and the capacitance of the measurement voltmeter place a practical limit on the maximum height of the measurement conductor.

It should be noted that radiated emissions of these boards were measured from 30 MHz to 1 GHz in a semianechoic chamber. An unterminated wire one meter in length was

attached to the far end of the set of reference lands to simulate the attachment of a cable shield. There appeared to be a correlation between a reduction in ground drop and a reduction in radiated emissions. Reductions in radiated emissions of some 10 dB were observed between configurations 1A and 1D from 30 MHz to about 60 MHz. Above this frequency, the reductions were not as substantial and were somewhat erratic. (Radiated emissions for configuration 1D were larger than those for 1A at some frequencies.) It is worth noting (as indicated in Figure 12) that the large and consistent differences in ground drop occurred below approximately 60 MHz. From 60 MHz to about 100 MHz, less of a difference between those is observed for all four configurations than was observed below 60 MHz. Perhaps this explains the ineffectiveness of ground lands in the reduction of measured radiated emissions above 60 MHz. Reduced ground drop may very well reduce radiated emissions. However, it should be realized that, as was shown in this paper, two different land patterns may exhibit quite different levels of ground drop over certain portions of the frequency spectrum and very little difference over other portions.

### **Acknowledgments**

This work was supported by the Information Products Division of IBM, Lexington, Kentucky. The author acknowledges the assistance of Lewis Alexander, an IBM Summer Associate, throughout the course of this work. The assistance of Stephen Parker, whose meticulous construction of the test boards and their terminations made possible the accurate prediction of the experimental results, is gratefully acknowledged. The author also gratefully acknowledges the support and encouragement by David Lee and George Alspaugh of the IBM facility at Lexington. A special note of recognition is due Albert Ruehli and Pierce Brennan of the IBM T. J. Watson Research Center at Yorktown Heights. New York, who provided helpful discussions and encouragement during the course of this work. Their pioneering work and insight in the development of the numerical techniques for computing land inductances and capacitances made this work possible.

### References

- "Computing Device," Federal Communications Commission Rules and Regulations, Vol. 2, Part 15, Subpart J, pp. 160–176, July 1981.
- H. W. Ott, "Controlling EMI by Proper Printed Wiring Board Layout," *Proceedings*, 1985 International Symposium and Technical Exhibition on Electromagnetic Compatibility, Zurich, Switzerland, March 1985.
- 3. R. F. German, "Use of a Ground Grid to Reduce Printed Circuit Board Radiation," *Proceedings*, 1985 International Symposium and Technical Exhibition on Electromagnetic Compatibility, Zurich, Switzerland, March 1985.
- C. R. Paul and D. R. Bush, "Radiated Emissions From Common-Mode Currents," *Proceedings*, 1987 IEEE International Symposium on Electromagnetic Compatibility, Atlanta, GA, August 1987.

- H. W. Ott, "Ground—A Path for Current Flow," Proceedings, 1979 IEEE International Symposium on Electromagnetic Compatibility, San Diego, CA, October 1979.
- H. W. Ott, "Digital Circuit Grounding and Interconnection," Proceedings, 1981 IEEE International Symposium on Electromagnetic Compatibility, Boulder, CO, August 1981.
- C. R. Paul, "Printed Circuit Board Crosstalk," *Proceedings*, 1985
  IEEE International Symposium on Electromagnetic
  Compatibility, Wakefield, MA, August 1985.
- C. R. Paul, "Applications of Multiconductor Transmission Line Theory to the Prediction of Cable Coupling, Vol. I, Multiconductor Transmission Line Theory," *Technical Report RADC-TR-76-101*, Rome Air Development Center, Griffiss AFB, NY, April 1976.
- W. T. Weeks, A. J. Jimenez, G. W. Mahoney, D. Mehta, H. Qassemzadeh, and T. R. Scott, "Algorithms for ASTAP—A Network-Analysis Program," *IEEE Trans. Circuit Theor.* CT-20, 628-634 (November 1973).
- A. E. Ruehli, "Equivalent Circuit Models for Three-Dimensional Multiconductor Systems," *IEEE Trans. Microwave Theor. Tech.* MTT-22, No. 3, 216–221 (March 1974).
- P. A. Brennan, N. Raver, and A. E. Ruehli, "Three-Dimensional Inductance Computations with Partial Element Equivalent Circuits," *IBM J. Res. Develop.* 23, No. 6, 661–668 (November 1979)
- A. E. Ruehli, "Survey of Computer-Aided Electrical Analysis of Integrated Circuit Interconnections," *IBM J. Res. Develop.* 23, No. 6, 626-639 (November 1979).
- C. R. Paul and S. A. Nasar, Introduction to Electromagnetic Fields, Second Edition, McGraw-Hill Book Co., Inc., New York, 1987.
- A. E. Ruehli, "Inductance Calculations in a Complex Integrated Circuit Environment," *IBM J. Res. Develop.* 16, No. 5, 470–481 (September 1972).
- F. W. Grover, *Inductance Calculations*, Dover Publications, New York, 1946.
- W. T. Weeks, L. L. Wu, M. F. McAllister, and A. Singh, "Resistive and Inductive Skin Effect in Rectangular Conductors," *IBM J. Res. Develop.* 23, No. 6, 652–660 (November 1979).
- P. Silvester, "Modal Network Theory of Skin Effect in Flat Conductors," *Proc. IEEE* 54, No. 9, 1147–1151 (September 1966)
- C. Hoer and C. Love, "Exact Inductance Equations for Rectangular Conductors with Applications to More Complicated Geometries," J. Res. Nat. Bureau of Standards—C. Eng. Instrum. 69C, No. 2, 127–137 (April–June 1965).
- A. E. Ruehli and P. A. Brennan, "Efficient Capacitance Calculations for Three-Dimensional Multiconductor Systems," *IEEE Trans. Microwave Theor. Tech.* MTT-21, 76-82 (February 1973).
- A. E. Ruehli and P. A. Brennan, "Capacitance Models for Integrated Circuit Metallization Wires," *IEEE J. Solid-State Circuits* SC-10, No. 6, 530–536 (December 1975).
- C. R. Paul and A. E. Feather, "Computation of the Transmission Line Inductance and Capacitance Matrices from the Generalized Capacitance Matrix," *IEEE Trans. Electromag.* Compat. EMC-18, No. 4, 175–183 (November 1976).
- S. Ramo, J. R. Whinnery, and T. VanDuzer, Fields and Waves in Communication Electronics, John Wiley, Inc., New York, 1965
- C. S. Yen, Z. Fazarinc, and R. L. Wheeler, "Time-Domain Skin-Effect Model for Transient Analysis of Lossy Transmission Lines," *Proc. IEEE* 70, No. 7, 750–757 (July 1982).
- C. R. Paul, "Solution of the Transmission Line Equations for Three-Conductor Lines in Homogeneous Media," *IEEE Trans. Electromag. Compat.* EMC-20, No. 1, 216–222 (February 1972)
- C. R. Paul, "Applications of Multiconductor Transmission Line Theory to the Prediction of Cable Coupling, Vol. VII, Digital Computer Programs for the Analysis of Multiconductor

Transmission Lines," *Technical Report RADC-TR-76-101*,
Rome Air Development Center, Griffiss AFB, NY, July 1977.
26. H. H. Skilling, *Electric Transmission Lines*, McGraw-Hill Book Co., Inc., New York, 1951, Ch. 6.

Received August 18, 1986; accepted for publication September 20, 1988 Clayton R. Paul Department of Electrical Engineering, University of Kentucky, Lexington, Kentucky 40506. Dr. Paul is a Professor of Electrical Engineering at the University of Kentucky. He received his B.S. degree in 1963 from The Citadel, Charleston, South Carolina, his M.S. degree in 1964 from the Georgia Institute of Technology, Atlanta, and his Ph.D. degree in 1970 from Purdue University, Lafayette, Indiana, all in electrical engineering. In 1987 he was elected a Fellow of the Institute of Electrical and Electronics Engineers for contributions to the understanding and modeling of crosstalk in cable assemblies. His general area of research interest involves electromagnetic compatibility, with emphasis on the modeling and prediction of electromagnetic properties of electronic systems. He is the author of 70 technical papers, two textbooks on electric circuit theory.